Combustion regime transition of H2 flames during steady and transient operation of a sequential combustor

Author(s):
Solana Pérez, Roberto; Shcherbanev, Serge; Dharmaputra, Bayu; Ciani, Andrea; Noiray, Nicolas

Publication date:
2023

Permanent link:
https://doi.org/10.3929/ethz-b-000598109

Originally published in:
Proceedings of the Combustion Institute 39(4), https://doi.org/10.1016/j.proci.2022.08.014

Funding acknowledgement:
820091 - ThermoacOustic instabilities contRol in sequential Combustion cHambers (EC)

Available online at www.sciencedirect.com

ScienceDirect

Proceedings of the Combustion Institute 39 (2023) 4335–4344

Proceedings of the Combustion Institute

www.elsevier.com/locate/proci

Combustion regime transition of H_2 flames during steady and transient operation of a sequential combustor

Roberto Solana-Pérez [a,*], Sergey A. Shcherbanev [a], Bayu Dharmaputra [a], Andrea Ciani [b], Nicolas Noiray [a,*]

[a] *CAPS Laboratory, Department of Mechanical and Process Engineering, ETH Zürich, Switzerland*
[b] *Ansaldo Energia Switzerland AG, Baden 5401, Switzerland*

Received 5 January 2022; accepted 3 August 2022
Available online 30 September 2022

Abstract

The combustion regime transition in a sequential burner (SB) supplied with H_2 (48 kW) is experimentally studied during steady and transient operation. The test rig is a simplified model of an industrial sequential combustor featuring two-staged combustion chambers separated by a mixing section in which dilution air and fuel are injected. The temperature, velocity and composition of the hot vitiated gas flowing through the SB are defined by the products from the first stage (30 kW natural gas-air flame at equivalence ratio 0.7), and by the mass flow of dilution air $\dot{m}_{DA}$. To study the combustion regime transition during steady operation of the combustor, $\dot{m}_{DA}$ is fixed at several values between 22 g/s and 7 g/s. For transient operation investigations, $\dot{m}_{DA}$ is suddenly changed between 20 and 7 g/s, which triggers a fast transition of the combustion mode. High-speed hydroxyl radicals OH^* chemiluminescence is used to characterize the combustion process, and optical emission spectroscopy (OES) and tunable diode laser absorption spectroscopy (TDLAS) are respectively used to extract mean and time-resolved temperatures of the vitiated gas in the SB. In particular, we investigate the transition from a propagation-driven turbulent flame anchored at the inlet of the sequential combustion chamber, to a flame stabilized by autoignition inside the mixing section of the burner when the dilution air mass flow is suddenly reduced. Zero-dimensional (0D) simulations are used to analyze the underlying combustion regime transition. A 0D reactor network is developed and calibrated with the experimental data. This simplified low-order model predicts well the flame location for both steady and transient operation. Moreover, the good agreement between the numerical results and the experimental data demonstrates that time-resolved TDLAS successfully enables measurement of small temperature variations in the vitiated flow associated with non-perfect mixing of the different streams in the SB.

Keywords: Hydrogen; Autoignition; Sequential combustion

* Corresponding authors.
E-mail addresses: sroberto@ethz.ch (R. Solana-Pérez), noirayn@ethz.ch (N. Noiray).
https://doi.org/10.1016/j.proci.2022.08.014

1. Introduction

Supplying gas turbines with H_2 can drastically reduce carbon dioxide emissions and provide a solution to the energy storage problem of future networks based on the massive use of renewable sources and on power-to-gas-to-power technology. In gas turbines, the reheat (sequential) combustion concept offers high fuel and operational flexibility, and is particularly well-suited for highly reactive fuels like H_2 while keeping low emissions. These characteristics are thoroughly described in Pennell et al. [1], Güthe et al. [2], Bothien et al. [3], Ciani et al. [4], 5]. A key advantage of the reheat concept is that combustion in the sequential stage is defined by a complex balance between autoignition and propagation that is strongly dependent on the flow temperatures, and that can be effectively controlled. The complexity of this concept leads to a scarcity of studies on combustion of pure H_2 in reheat systems. Previous studies analysed flame stabilization mechanisms in sequential combustion chambers [6–12] but they were focusing on the combustion of natural gas and air in the sequential stage. In particular, it was shown that different combustion regimes, namely autoignition and flame propagation, can govern the flame stabilization [6] and that these regimes can coexist. These findings were confirmed with experiments [7] and other numerical simulations [8]. Fewer studies deal with H_2-rich fuels or pure H_2 used at reheat conditions. Some numerical investigations focused on 0D, 1D or simple geometrical configurations [13–15], and flame stabilization in second stage flames featuring a jet-in-crossflow configuration was studied in Solana-Pérez et al. [16], 17], where [16] used H_2-rich fuels. A series of experimental studies [18–20] were performed with a reheat combustor that shares common features with the academic combustor used in the present work. In the latter references, the combustion of H_2 diluted with N_2 in a high pressure sequential combustor was investigated, with a focus on the formation of autoignition kernels rather than on combustion regime transition. The effects of pressure increase on sequential flames at gas turbines relevant conditions was addressed in Brower et al. [21] using 0D/1D simulations, and in Gruber et al. [22] using LES. Recent numerical studies [22,23] were published where a H_2 sequential simplified configuration was simulated with DNS and LES. The authors studied the flame stabilization and also observed the coexistence of autoignition and propagation regimes, and the formation of spontaneous ignition events due to the high sensitivity to temperature variations. A recent experimental work [24] assessed the effects of mixing quality on the sequential flame dominant combustion regime and emissions. The experiments were conducted in the same experimental test rig as the current study.

There are important knowledge gaps about the transition of combustion regimes and its role on flame stabilization when pure H_2 is burned, and when the thermo-chemical conditions of the vitiated flow entering the sequential burner (SB) are changed. In this study the effect of such thermo-chemical changes on the combustion of H_2 in a generic sequential combustor is investigated. Firstly, temperature and composition of the hot stream are consecutively modified during steady operation of the combustor in order to study the flame stabilization mechanisms. This is done by changing the dilution air mass flow rates while the lean natural gas-air flame at the first stage is not modified. Secondly, the combustion regime transition is analysed during transient operation of the combustor while the vitiated flow temperature is abruptly decreased. These results are compared against a calibrated 0D reactor network model in the last part of this paper.

2. Experimental setup

The experiments are conducted in a generic sequential combustor operated at atmospheric pressure and featuring two axially staged combustion chambers separated by a mixing section and a SB in which dilution air and fuel are injected, see Fig. 1. The first stage consists of a 4x4 array of turbulent jet flames burning a technically premixed mixture of natural gas (NG) and air at lean conditions. The hot vitiated flow generated in the first stage is then diluted with fresh air at 300 K. The dilution air module transitions from 62×62 mm^2 to 25×38 mm^2 cross section and contains 4 large vortex generators (VGs). The SB features a high-speed mixing section with a cross section of 25×38 mm^2. It is equipped with the sequential fuel injector, that features a vertical aerodynamic symmetric profile with 2 opposing VGs. The nozzle outlet diameter is 2.4 mm, and its distance to the end of the mixing section is 180 mm. The H_2 injected from this nozzle mixes with the vitiated flow in the mixing section. Finally, the sequential combustion chamber has a cross section of 62×62 mm^2. The transition between the mixing section and the sequential combustion chamber is a sudden area expansion. The area of the combustion chamber outlet orifice is set to 1500 mm^2, which allows to prevent thermoacoustic instabilities. The operating conditions considered a constant power split of 30/48 kW between first and second stage at atmospheric pressure. A lean NG/air mixture at equivalence ratio $\phi_1 = 0.7$ is used in the first stage, delivering a hot vitiated flow that is then diluted with varying amounts of dilution air. For the steady operation, mass flow rates of dilution air range between $\dot{m}_{DA} = 7 - 22$ g/s, varying the flow temperature from 1150 K to 850 K, the velocity from 90 m/s to 105 m/s, and the global

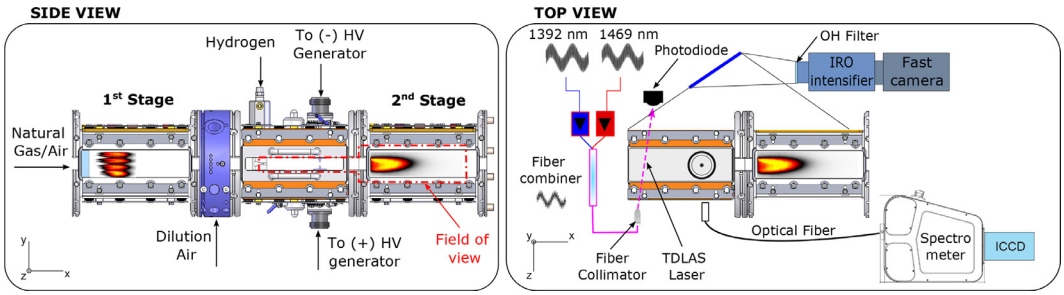

Fig. 1. Sequential combustor featuring a 1st stage combustion chamber with 4 × 4 premixed jet flames, a dilution air module, a sequential burner and a 2nd stage chamber. The field of view of OH* chemiluminescence images is shown with red dotted lines. (For interpretation of the references to color in this figure legend, the reader is referred to the web version of this article.)

equivalence ratios of the SB from 1.21 to 0.48 respectively in various steps. This global equivalence ratio takes into consideration the H_2, and the O_2 from both the dilution air stream and the first stage products. For the transient operation, only one sudden variation of $\dot{m}_{DA}$ is investigated, from 20 g/s to 7 g/s. Pure H_2 at 300 K is used as sequential fuel without any carrier gas. The residence time of the fuel in the mixing section is estimated to be between 1.5 and 2 ms based on the mean convective velocities.

2.1. Diagnostic techniques

High-speed line-of-sight integrated OH* chemiluminescence is performed to record the mixing section and the sequential combustion chamber, see Fig. 1. The camera frame rate is set to 10 kHz with a gate width of 40 μs, and the acquisition time is 1.5 s. A high-speed CMOS camera (LaVision star X) is used with a lens coupled high-speed intensifier (LaVision HS-IRO), equipped with a CERCO UV lens 45 mm, F/1.8, and a band-pass filter (Edmund Optics, centered at 310 nm, FWHM 10 nm).

Tunable diode laser absorption spectroscopy (TDLAS) technique is used to measure time-resolved temperatures (e.g. Goldenstein et al. [25]) in the vitiated flow of the SB. The measurements are single-point line-of-sight (LOS) integrated and were obtained at one single location with acquisition rate of 5 kHz. The horizontal laser beam ($x-z$ plane) crosses the SB laterally with an angle of 30 with respect to the z-axis to avoid spurious reflections and improve the signal to noise ratio (see Fig. 1). The center of this inclined laser beam is located 23 mm downstream (x-direction) from the sequential injector and 5 mm below (y-direction) the nozzle to obtain the temperature signal closest to the injector while avoiding interaction with the cold H_2 jet. Different vertical positions were not tested due to the symmetry of the test-rig upstream from the injector. Only the transient operation is measured with this technique. The TDLAS setup consists of two infrared diode lasers (DFB-NEL) centered at 1392 nm and 1469 nm which are probing the absorption spectra of water vapour (H_2O molecule) at 7185.59 cm^{-1} and 6806.03 cm^{-1}. The lasers are injection-current tuned by laser diode controllers (LDC 501m), which are modulated by a function generator (Tektronix AFG31000). The lasers emitting near 1392 nm and 1469 nm are sinusoidally scanned at 5 kHz and modulated at 150 kHz and 200 kHz with modulation depths of 0.09 cm^{-1} and 0.092 cm^{-1} respectively. The laser beams from both lasers are then combined with a fiber combiner and subsequently collimated to a beam diameter of 3 mm with a fiber collimator (Thorlabs F280APC-C). The collimated beam is then detected by a photodiode (Thorlabs PDA05CF2). The signal of the photodiode is sampled at 10 MS/s with a 16-bit data acquisition card (GaGe). The WMS-2f and 1f signals are extracted by demodulating the signal at the modulation frequencies of the lasers. Temperature along the TDLAS LOS is inferred following [26]. More detailed description of the method can be found in Dharmaputra et al. [27].

Optical emission spectroscopy (OES) of single 10-nanosecond non-equilibrium plasma (NEP) discharge is used to obtain the temperature of the vitiated flow inside the mixing section without the addition of sequential fuel to avoid the effect of the flame. For these OES measurements, two pin electrodes are inserted inside the mixing section 103 mm downstream of the fuel injector from top and bottom to create the NEP discharges using a high voltage (HV) generator, and later removed for the combustion measurements. The spatially-integrated and time-resolved optical emission is collected and transmitted through an optical fiber with a transmission from 190 to 1100 nm to the entrance slit of the IsoPlane-320 (Princeton Instruments) spectrometer with 1800 I/mm diffraction grating associated with the intensified PI-MAX4 camera. Emission spectra of the second positive system of molecular nitrogen, corresponding to the

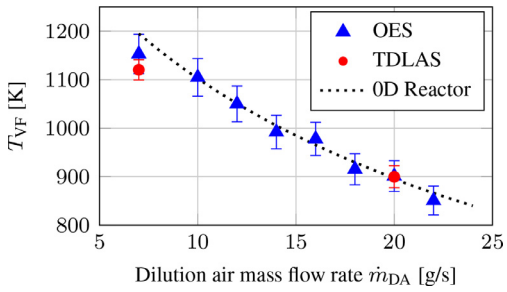

Fig. 2. Temperature of vitiated flow measured at mixing section for various dilution air mass flow rates at steady operation of the test rig. Experimental temperatures from OES (blue triangles), and TDLAS (red circles), and numerical values from the calibrated 0D reactor network (dotted line). (For interpretation of the references to color in this figure legend, the reader is referred to the web version of this article.)

electronic transition $C^3\Pi_u \rightarrow B^3\Pi_g$ are acquired. The excitation energy of the upper electronic state ($C^3\Pi_u$) is 10.8 eV. The excitation in the discharge region is produced within direct electron impact processes from the ground state of N_2. More details of this method can be found in [28]. The amplitude of applied high-voltage pulses is tuned in order to obtain a discharge initiation in a glow regime. Glow nanosecond NEP discharges have negligible thermal effect.

3. Results and discussion

3.1. Steady operation

In these experiments the mass flow of the dilution air is modified consecutively and each operating point is recorded separately. Fig. 2 shows the mean temperatures of the vitiated flow T_{VF} inside the mixing section as function of the mass flow rate of dilution air $\dot{m}_{DA}$. Experimental values measured with OES (blue triangles with ±35 K total error), and time-averaged values from TDLAS (red circles with ±25 K standard deviation) show very good agreement.

Fig. 3 presents LOS integrated OH^* intensity fields of the SB mixing section and of the combustion chamber. Fig. 3-left shows the time-averaged fields over 10000 images and 1 second of measurement for various dilutions air mass flow rates. Three different anchoring dynamics are observed: i) flames anchored at the inlet of the sequential combustion chamber at "cold" conditions with $\dot{m}_{DA} =$ 20, 22 g/s; ii) flames stabilized inside the mixing section at different distances from the injector nozzle at "hot" conditions with $\dot{m}_{DA} = 7, 12$ g/s; and iii) coexistence of the previous 2 anchoring dynamics at "mild" conditions with $\dot{m}_{DA} = 16$ g/s. Fig. 3-right is a time sequence of instantaneous OH^* fields corresponding to $\dot{m}_{DA} = 16$ g/s. The sequence shows an instance of the transition between flames anchored at the combustion chamber and flames stabilized in the mixing section. The transition is caused by the random appearance of spontaneous ignition events (blue circles) and disappearance of the flame in the combustion chamber, leading to the coexistence of both types of flames. See [24] for a detailed analysis of the spontaneous ignition events.

A 0D reactor network is developed using Cantera [29] with San Diego mechanism [30] in order to study the conditions at which autoignition and flame propagation govern the combustion process in the sequential combustor, see Fig. 4. The network model consists of 3 stages: a) first stage flame is simulated using chemical equilibrium at constant pressure and enthalpy of a CH_4/Air mixture. The required inputs include pressure, gases temperatures, kinetic mechanism, and equivalence ratio. A 0D batch reactor with wall heat losses is introduced to simulate experimental wall losses; b) dilution air is added to the vitiated flow in a perfect mixing process; c) sequential H_2 fuel is added in a partial mixing process as function of a mixture fraction parameter (Z) between the fresh fuel and the vitiated flow, and a 0D adiabatic batch reactor at constant pressure is used to ignite the resulting reactive vitiated flow. The 0D reactors are homogeneous, closed, and have a moving wall to ensure the constant pressure of the system. The autoignition delay is computed from the last batch reactor as the time where the highest temperature gradient is found. The simplified model simulates each stage of the sequential combustor operated at atmospheric pressure, and it is calibrated by introducing heat losses at the first stage to match the temperatures measured with OES and TDLAS.

The temperature results are shown in Fig. 2 matching well the experimental data. Several simulations are performed varying two parameters: i) the temperature of the vitiated flow T_{VF} by modifying the concentration of dilution air, and ii) the mixture fraction parameter Z that defines the mixing between the pure H_2 jet at 300 K ($Z = 1$), and the hot vitiated gas, i.e. the stream containing the hot products from first stage and the dilution air ($Z = 0$). Note that changes in the vitiated flow temperature are caused by different concentrations of fresh dilution air and hot products from the first stage flame. By doing so, the reactor network takes into account changes in both temperature and composition between the three streams (hot products from the first stage, dilution air, and sequential fuel). Fig. 5-top shows autoignition delay times τ_{AI} as function of the mixture fractions Z for various T_{VF}. The most reactive mixture fraction Z_{mr} is denoted with diamond markers, and it is defined as the mixture

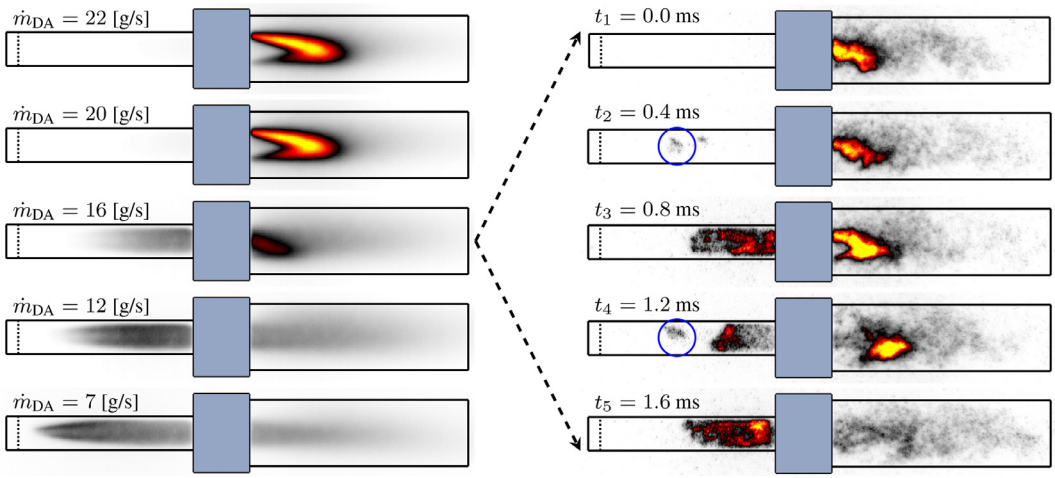

Fig. 3. Left: Time-averaged OH* intensity fields for various mass flow rates of dilution air; Right: excerpt of case $\dot{m}_{DA} =$ 16 g/s showing instantaneous OH* images of the erratic transitions from flames anchored at the SB outlet (t_1) to flames stabilized inside the SB mixing section (t_5) in the form of spontaneous ignition kernels. The dotted vertical lines show the nozzle location.

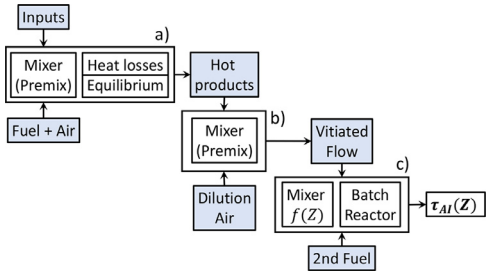

Fig. 4. Schematic of 0D reactor network model using Cantera modules. a) First stage, b) dilution air, and c) sequential burner modules. Autoignition delays are the output.

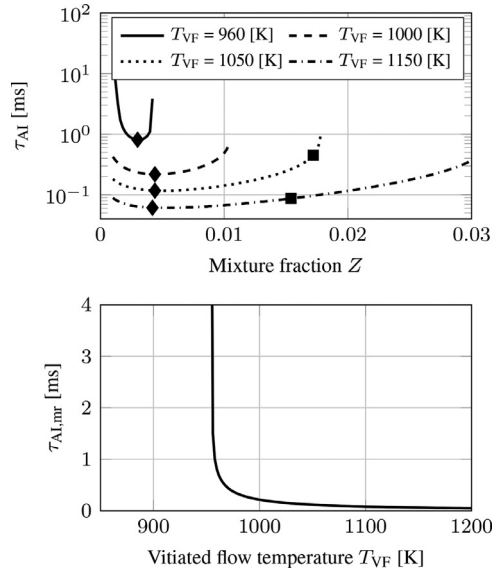

Fig. 5. Top: Autoignition delays τ_{AI} as function of mixture fraction Z between vitiated flow ($Z = 0$) and hydrogen ($Z = 1$) for various vitiated flow temperatures T_{VF}. Diamond and square symbols respectively show the most reactive mixture fractions (Z_{mr}) and the stoichiometric conditions. Bottom: Autoignition delays $\tau_{AI,mr}$ at most reactive conditions (Z_{mr}, diamond markers from Top) as function of the vitiated flow temperature.

fraction that exhibits the shortest autoignition delay at each vitiated flow temperature, see [31]. This value is found at very lean mixture compositions, with equivalence ratios of $\phi_{mr} \simeq 0.2$–0.3. The so-called most reactive autoignition times $\tau_{AI,mr}$ show a reduction of more than one order of magnitude for the range of T_{VF} of interest. The exponential dependence between $\tau_{AI,mr}$ and T_{VF} is shown in Fig. 5-bottom. Previously defined "hot" regime ($\dot{m}_{DA} = 7, 12$ g/s) is associated with autoignition delays much smaller than the residence time in the SB mixing section ($\tau_{AI} < 0.2$ ms); "cold" regime ($\dot{m}_{DA} = 20, 22$ g/s) shows that autoignition delays are larger than the residence time, hence autoignition is not expected in the mixing section ($\tau_{AI} > 2$ ms); and "mild" regime ($\dot{m}_{DA} = 16$ g/s) is associated with large gradients of autoignition delays for varying temperatures. This can be observed comparing Figs. 5-bottom and 2.

Fig. 6 compares the experimental averaged flame presence (color map representing OH* averaged intensity) and the autoignition lengths computed from the most reactive autoignition delays

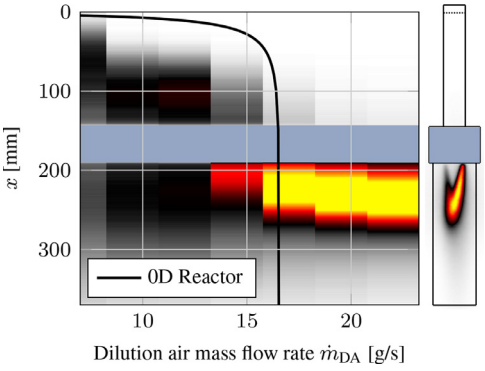

Fig. 6. Time-averaged OH* intensity integrated in the y-direction along the mixing section (x from 0 to 180 mm) and combustion chamber (from 180 to 370 mm) for various $\dot{m}_{DA}$. The solid line represents the autoignition lengths from the calibrated 0D reactor network. Fuel injector at $x = 0$.

of the 0D reactor model (black solid line) for various dilution air mass flow rates. The three temperature regimes previously mentioned can be observed in this figure. At so-called "cold" conditions ($\dot{m}_{DA} > 18$ g/s) the flame only appears anchored at the combustor inlet. The autoignition lengths computed from the 0D reactor (solid line) are far downstream from the actual flame front. This indicates that these flames are anchored by flame-propagation mechanism thanks to the recirculation of hot gas at the inlet of the combustion chamber, similarly to [8,23]. A further decrease of the vitiated flow temperatures does not affect the flame anchoring as it is not dominated by autoignition. At "hot" conditions ($\dot{m}_{DA} < 12$ g/s) the flame is always stabilized by autoignition inside the SB mixing section, in agreement with the 0D model. Finally, at "mild" conditions ($\dot{m}_{DA} = 12 - 18$ g/s) coexistence of flame inside the mixing section and at the combustion chamber inlet is observed. At these conditions, the predicted autoignition location is close to the end of the mixing section. At the same time, these temperatures are associated with large gradients of $\tau_{AI,mr}$ as shown in Fig. 5-bottom. This means that small local temperature variations due to non-perfect mixing of the vitiated flow can lead to autoignition length displacements sufficiently large to push the flame front outside the mixing section, promoting a change of the flame stabilization mechanism. As an example, at $\dot{m}_{DA} =$ 16 g/s, temperature variations similar to those measured with TDLAS, i.e. $\Delta T_{VF} \simeq 50$ K, can lead to $\Delta\tau_{AI,mr} \simeq 0.7$ ms, and estimated autoignition displacements of $\Delta x_{AI} = 70$ mm that are sufficient to delay ignition to the combustion chamber.

The 0D reactor network model was also used to assess the impact of the first stage fuel on the autoignition properties of the sequential stage.

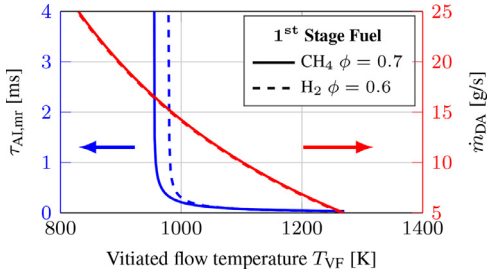

Fig. 7. Autoignition delays $\tau_{AI,mr}$ at most reactive conditions (blue left), and vitiated flow temperatures at each dilution air mass flow $\dot{m}_{DA}$ when using CH_4 or H_2 as first stage fuel.. (For interpretation of the references to color in this figure legend, the reader is referred to the web version of this article.)

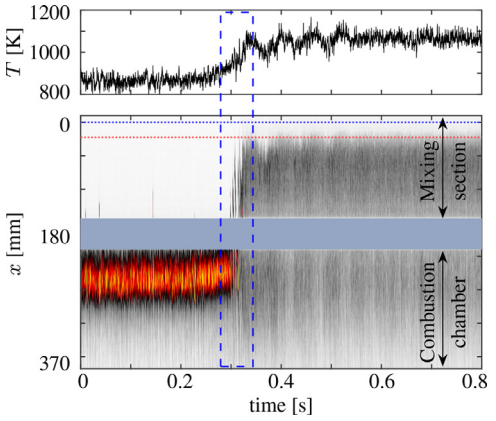

Fig. 8. Top: TDLAS temperature signal. Bottom: Instantaneous OH* intensity integrated in the y-direction and stitched together in time during transient operation from $\dot{m}_{DA} = 20$ g/s to 7 g/s. Dotted lines show TDLAS probe (red, 23 mm) and injector nozzle (blue, 0 mm). (For interpretation of the references to color in this figure legend, the reader is referred to the web version of this article.)

Fig. 7 shows the autoignition delays at most reactive conditions $\tau_{AI,mr}$ of the sequential stage (blue left curves) when firing the first stage with CH_4 or H_2. It also shows the temperature of the vitiated flow at each operating point of $\dot{m}_{DA}$ (red right curves). The equivalence ratio of the first stage H_2 case was chosen such that the temperature of the vitiated flow (red right curves) matches the CH_4 case, allowing to compare the autoignition properties of the sequential stage purely based on mixture composition of the vitiated flow. In this case, modifying the first stage fuel would change the composition of the hot vitiated products concentration (mainly CO_2 and H_2O). The results show that burning H_2 in the first stage would slightly delay the onset of autoignition to higher temperatures compared to the CH_4 case. However, this delay is rather small and could be easily tuned by slight variations of the vi-

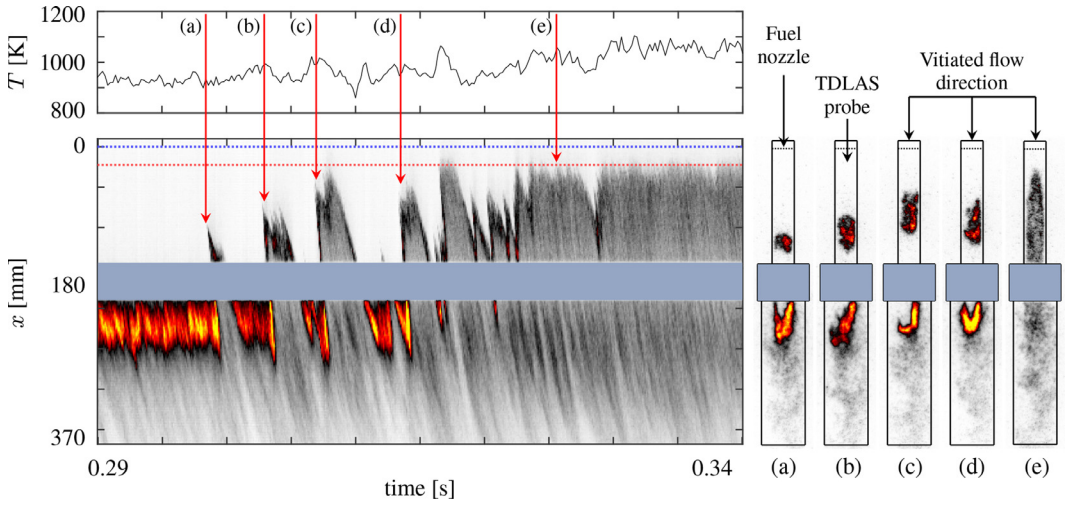

Fig. 9. Left: Zoomed region inside blue dashed rectangle in Fig. 8 centered at transition of flame anchoring. Right: Instantaneous OH* fields extracted at the time instants marked on the temperature plot, showing consecutive spontaneous ignition events (a,b,c,d) finally leading to transition of flame stabilization location (e). (For interpretation of the references to color in this figure legend, the reader is referred to the web version of this article.)

tiated flow temperatures. As a conclusion, it is not expected that the use of H_2 in the first stage will have a major influence on the dominant combustion regimes of the second stage.

3.2. Transient operation

The transition from a H_2 flame anchored at the combustion chamber inlet to a flame stabilized inside the SB mixing section during transient operation of the combustor is analysed in this section using synchronized measurements of OH* chemiluminescence and TDLAS. Several tests are performed changing the dilution air mass flow rate from $\dot{m}_{DA} = 20$ g/s to $\dot{m}_{DA} = 7$ g/s. Fig. 8 displays the results for one of the transient tests. The top plot shows the time-resolved temperatures of the hot vitiated flow obtained with TDLAS at 5 kHz. The temperature significantly increases when the dilution air mass flow is suddenly reduced. This temperature increase starts at $t \sim 0.25$ s, lasts about 100 ms, and is followed by decaying oscillations until it stabilizes at $t \sim 0.6$ s. The bottom plot of Fig. 8 presents the time evolution of the radially integrated values of OH* intensity recorded at 10 kHz along the mixing section ($x = 0$–180 mm) and the combustion chamber ($x = 180$–370 mm). The flame appears anchored at the combustion chamber inlet while $T \sim 900$ K. Sudden transition occurs at $t \sim 0.30$ s, lasting about 30 ms, and leading to a flame stabilized inside the mixing section. Note how the oscillations that follow the temperature increase affect the flame front location in the chemiluminescence results.

A more detailed view of the transition is shown in Fig. 9. The plots on the left display the time window enclosed in the blue dashed box of Fig. 8 with a total duration of 50 ms centered at the transition event. The figure shows a sequence of consecutive spontaneous ignition events bursting inside the mixing section right after localized temperature peaks, see temperature signal markers. The duration of the shortest AI kernels bursts is of the order of 2 ms. The estimated delay between TDLAS and OH* signals is of the order of 0.1 ms, i.e. one order of magnitude smaller than the characteristic time of any recorded phenomena. This means that TDLAS and chemiluminescence data are fully resolved in time.

The first autoignition kernels in Fig. 9 appear isolated and fail to stabilize the flame. They are flushed downstream to the combustion chamber, causing the blow-off and later re-ignition of the flame anchored at the combustor inlet. As mean temperature increases, the ignition events become more frequent and lead to a new flame front continuously stabilized inside the mixing section, and to the complete extinction of the flame anchored in the sequential combustion chamber. These results show that the displacement of the flame front is caused by a transition of the dominant combustion regime from propagation to autoignition. The flame front does not propagate upstream from the combustor inlet, instead new flames autoignite and stabilize inside the mixing section. The right plot of Fig. 9 features line-of-sight integrated OH* intensity fields that show several instants with spontaneous ignition events in the SB mixing section.

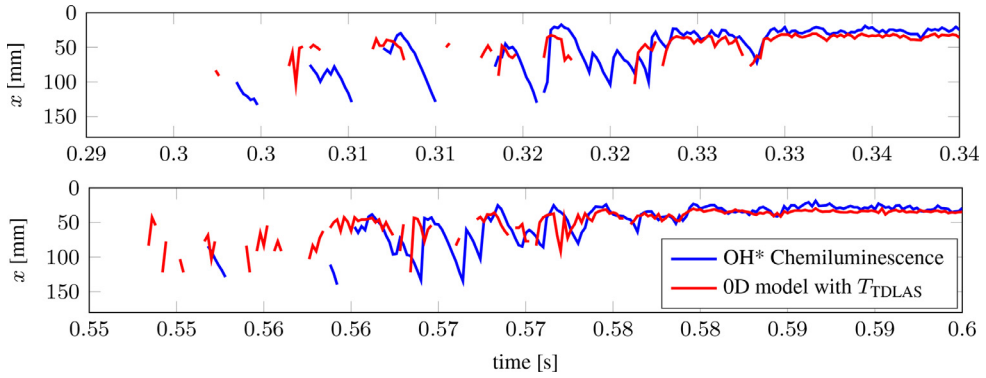

Fig. 10. Flame front displacement from combustor inlet to mixing section. Blue: Experimental flame front detected from OH* luminosity plots. Red: Autoignition locations computed with the 0D reactor network model using the TDLAS instantaneous temperatures. Two experimental tests are shown (top and bottom). Fig. 9 corresponds to top. (For interpretation of the references to color in this figure legend, the reader is referred to the web version of this article.)

They show the ignition of the kernels closer to the fuel injector for increasing local peak temperatures (a,b,c,d) and the final stabilized flame (e).

The TDLAS probe measures the temperature of the vitiated gas resulting from the mixing process between the hot products of the first stage flame and the dilution air stream. Two questions remain, i) whether the single-point and line-of-sight integrated TDLAS signal successfully captures actual local temperature fluctuations caused by non-perfect mixing of the hot vitiated flow; and ii) whether these local temperature fluctuations associated with the mixing quality affect the stabilization of the sequential flame. In order to investigate this, the TDLAS temperature signal is introduced as an input in the calibrated 0D reactor network model previously described. The target is to use this simplified low-order model to compute the autoignition delays and the autoignition lengths associated with the measured temperatures of the vitiated flow. Fig. 10 shows the results of this analysis centered at the transition event. The red curves represent the estimated flame location computed with the 0D reactor network model that used the TDLAS temperature signal as input to compute autoignition delays at most reactive conditions. The blue curves show the actual flame front location extracted from the OH* chemiluminescence fields. Two different test runs are shown (bottom and top plots) under the same operating conditions for better corroboration. The time shift between both cases is caused by the acquisition setup not being synchronized with the dilution air change. Nevertheless, this has no effect on the results, as they represent the same phenomena just shifted in time. The results of Fig. 10 show good agreement. The experimental flame front location (blue) correlates well with the autoignition location computed from 0D model (red). This demonstrates that the TDLAS technique successfully measures instantaneous local variations of the vitiated flow temperature. It also shows the high sensitivity of the autoignition flame to these temperature fluctuations related to the mixing quality, as they largely define the flame stabilization location. It should be noted that the fluctuations measured with TDLAS are associated with local variations of both temperature and gas composition. The vitiated flow is the result of the mixing between the hot products of the first stage and the cold dilution air. However, the mixing quality between these two streams can only be assumed partially premixed, i.e. lower temperatures are associated with higher concentration of dilution air, while higher temperatures are associated with higher concentration of combustion products from the first stage flame. This translates to local variations of temperature and species concentration (oxygen, radicals and other combustion products), that are expected to play a very important role on the definition of the autoignition properties. It is important to stress that the 0D reactor network model takes into account the mixing quality effect, i.e. the mixture composition variations associated with temperature fluctuations of the vitiated flow.

As final comments, it can be noted that the 0D model of the combustor, whose heat losses were adjusted to match the SB inlet temperature, is in good agreement with the experimental observations although the effects of turbulence and non-perfect mixing are not accounted for. It thus shows that such calibrated 0D model, which obviously cannot predict the flame dynamics, can however be a useful tool to make first assessments about the dominant combustion regimes to be expected in the combustor when composition or temperature are changed.

4. Conclusions

The combustion regime transition of pure H_2 flames in a sequential combustor test rig is experimentally investigated during steady and transient operation. The test rig features a lean natural gas-air flame in the first stage, and a pure H_2 flame in the sequential stage. Chemiluminescence of hydroxyl radicals is used to extract line-of-sight integrated information of the sequential flame, while mean and time-resolved temperatures of the hot vitiated flow are acquired using OES and TDLAS respectively. Variations of the vitiated flow temperature, velocity and composition are carried out by modifying dilution air mass flows in order to assess its effect on the dominant combustion regime of the sequential flame. The results of the steady operation show three types of flame stabilization regimes: i) flames anchored by turbulent premixed-flame propagation mechanism at the inlet of the combustion chamber at cold SB conditions, ii) flames stabilized by autoignition inside the SB mixing section at hot conditions, and iii) coexistence of the previous 2 types of flames and dominant combustion regimes at mild conditions. The mean temperature of the vitiated flow is acquired and validated with OES, TDLAS and a calibrated 0D reactor simulation, showing very good agreement. It is shown that the 0D reactor model can also be reliably used to estimate the three flame anchoring regimes for varying temperatures. The 0D reactor model also showed that using H_2 as the first stage fuel would not have strong effects on the dominant combustion regime of the sequential flame. The transient experiments demonstrate the capabilities of the TDLAS technique in the acquisition of time-resolved temperature measurements in sequential combustors. It is shown that the transition between a flame anchored at the combustor inlet to a flame stabilized inside the mixing section occurs abruptly and due to spontaneous autoignition events bursting in the mixing section that cause the extinction of the former flame, and the stabilization of the latter. The signal acquired with TDLAS is inserted into the 0D reactor network model to compute the autoignition delay times associated with the measured temperatures. The results give estimated time-resolved flame autoignition locations showing very high correlation with the actual flame front location observed with OH^* chemiluminescence. This demonstrates that TDLAS successfully captures local temperature fluctuations of the flow associated with non-perfect mixing, and that these fluctuations strongly affect the flame stabilization.

Declaration of Competing Interest

The authors declare that they have no known competing financial interests or personal relationships that could have appeared to influence the work reported in this paper.

Acknowledgments

Financial support of the Swiss Federal Office of Energy under the research project ARCH (No: SI/501781-01) and of the European Research Council under the ERC Consolidator Grant TORCH (No. 820091) are gratefully acknowledged.

References

[1] D.A. Pennell, M.R. Bothien, A. Ciani, et al., An introduction to the Ansaldo GT36 constant pressure sequential combustor, in: ASME Turbo Expo, 2017, pp. GT2017–64790.
[2] F. Güthe, J. Hellat, P. Flohr, The reheat concept: the proven pathway to ultralow emissions and high efficiency and flexibility, J. Eng. Gas Turbines Power 131 (2) (2008) 021503.
[3] M.R. Bothien, A. Ciani, J.P. Wood, G. Fruechtel, Toward decarbonized power generation with gas turbines by using sequential combustion for burning hydrogen, J. Eng. Gas Turbines Power 141 (12) (2019) 121013.
[4] A. Ciani, M.R. Bothien, B. Bunkute, J.P. Wood, G. Fruchtel, Superior fuel and operational flexibility of sequential combustion in Ansaldo Energia gas turbines, J. Glob. Power Propuls. Soc. 3 (2019) 630–638.
[5] A. Ciani, J.P. Wood, A. Wickström, et al., Sequential combustion in Ansaldo Energia gas turbines: the technology enabler for CO_2-free, highly efficient power production based on hydrogen, in: ASME Turbo Expo, 2020, pp. GT2020–14794.
[6] O. Schulz, N. Noiray, Autoignition flame dynamics in sequential combustors, Combust. Flame 192 (2018) 86–100.
[7] D. Ebi, U. Doll, O. Schulz, Y. Xiong, N. Noiray, Ignition of a sequential combustor: evidence of flame propagation in the autoignitable mixture, Proc. Combust. Inst. 37 (4) (2019) 5013–5020.
[8] O. Schulz, N. Noiray, Combustion regimes in sequential combustors: flame propagation and autoignition at elevated temperature and pressure, Combust. Flame 205 (2019) 253–268.
[9] P. Habisreuther, F.C.C. Galeazzo, C. Prathap, N. Zarzalis, Structure of laminar premixed flames of methane near the auto-ignition limit, Combust. Flame 160 (12) (2013) 2770–2782.
[10] A. Krisman, C. Mounaïm-Rousselle, R. Sivaramakrishnan, J.A. Miller, J.H. Chen, Reference natural gas flames at nominally autoignitive engine-relevant conditions, Proc. Combust. Inst. 37 (2) (2019) 1631–1638.
[11] F.M. Berger, T. Hummel, P. Romero Vega, B. Schuermans, T. Sattelmayer, A novel reheat combustor experiment for the analysis of high-frequency flame dynamics: concept and experimental validation, in: ASME Turbo Expo, 2018, pp. GT2018–77101.

[12] M. Zellhuber, C. Meraner, R. Kulkarni, W. Polifke, B. Schuermans, Large eddy simulation of flame response to transverse acoustic excitation in a model reheat combustor, J. Eng. Gas Turbines Power 135 (9) (2013) 091508.
[13] M. Poyyapakkam, J. Wood, S. Mayers, A. Ciani, F. Güthe, K. Syed, Hydrogen combustion within a gas turbine reheat combustor, ASME Turbo Expo, 2012, pp. GT2012–69165.
[14] T. Wind, F. Güthe, K. Syed, Co-firing of hydrogen and natural gases in lean premixed conventional and reheat burners (Alstom GT26), ASME Turbo Expo, 2014, pp. GT2014–25813.
[15] A. Gruber, M.R. Bothien, A. Ciani, K. Aditya, J.H. Chen, F.A. Williams, Direct numerical simulation of hydrogen combustion at auto-ignitive conditions: ignition, stability and turbulent reaction-front velocity, Combust. Flame 229 (2021) 111385.
[16] R. Solana-Pérez, L. Miniero, S. Shcherbanev, M. Bothien, N. Noiray, Morphology and dynamics of a premixed hydrogen-methane-air jet flame in hot vitiated turbulent crossflow, in: ASME Turbo Expo, 2020, pp. GT2020–16282.
[17] R. Solana-Pérez, O. Schulz, N. Noiray, Simulation of the self-ignition of a cold premixed ethylene-air jet in hot vitiated crossflow, Flow Turbul. Combust. 106 (4) (2021) 1295–1311.
[18] J.M. Fleck, P. Griebel, A.M. Steinberg, M. Stöhr, M. Aigner, A. Ciani, Experimental investigation of a generic, fuel flexible reheat combustor at gas turbine relevant operating conditions, in: ASME Turbo Expo, 2010, pp. GT2010–22722.
[19] J.M. Fleck, P. Griebel, A.M. Steinberg, C.M. Arndt, C. Naumann, M. Aigner, Autoignition of hydrogen/nitrogen jets in vitiated air crossflows at different pressures, Proc. Combust. Inst. 34 (2) (2013) 3185–3192.
[20] C.A. Schmalhofer, P. Griebel, M. Aigner, Influence of autoignition kernel development on the flame stabilisation of hydrogen-nitrogen mixtures in vitiated air of high temperature, in: ASME Turbo Expo, 2018, pp. GT2018–75483.
[21] M. Brower, E.L. Petersen, W. Metcalfe, H.J. Curran, M. Füri, G. Bourque, N. Aluri, F. Güthe, Ignition delay time and laminar flame speed calculations for natural gas/hydrogen blends at elevated pressures, J. Eng. Gas Turbines Power 135 (2) (2013) 021504.
[22] A. Gruber, T. Heggset, M. Duesing, A. Ciani, A numerical investigation of reheat hydrogen combustion in a simplified geometrical configuration from atmospheric pressure to full load conditions, in: ASME Turbo Expo, 2022, pp. GT2022–83218.
[23] K. Aditya, A. Gruber, C. Xu, T. Lu, A. Krisman, M.R. Bothien, J.H. Chen, Direct numerical simulation of flame stabilization assisted by autoignition in a reheat gas turbine combustor, Proc. Combust. Inst. 37 (2) (2019) 2635–2642.
[24] R. Solana-Pérez, S.A. Shcherbanev, A. Ciani, N. Noiray, Effect of mixing on the anchoring and combustion regimes of pure hydrogen flames in sequential combustors, J. Eng. Gas Turbines Power, 2022. GTP-22-1346, doi:10.1115/1.4055509. In press.
[25] C. Goldenstein, R. Spearrin, I. Schultz, J. Jeffries, R. Hanson, Wavelength-modulation spectroscopy near 1.4 μmfor measurements of H_2O and temperature in high-pressure and-temperature gases, Meas. Sci. Technol. 25 (5) (2014) 055101.
[26] G.B. Rieker, J.B. Jeffries, R.K. Hanson, Calibration-free wavelength-modulation spectroscopy for measurements of gas temperature and concentration in harsh environments, Appl. Opt. 48 (29) (2009) 5546–5560.
[27] B. Dharmaputra, S.A. Shcherbanev, A. Blondé, B. Schuermans, N. Noiray, Entropy transfer function measurement with tunable diode laser absorption spectroscopy, Proc. Combust. Inst. (2022), doi:10.1016/j.proci.2022.07.083.
[28] C.O. Laux, T. Spence, C. Kruger, R. Zare, Optical diagnostics of atmospheric pressure air plasmas, Plasma Sources Sci. Technol. 12 (2) (2003) 125.
[29] D. Goodwin, H. Moffat, R. Speth, Cantera: An Object-Oriented Software Toolkit for Chemical Kinetics, Thermodynamics, and Transport Processes, Caltech, Pasadena, CA, 2009.
[30] F. Williams, Chemical-Kinetic Mechanisms for Combustion Applications, San Diego University of California, 2010. http://combustion.ucsd.edu
[31] E. Mastorakos, T. Baritaud, T. Poinsot, Numerical simulations of autoignition in turbulent mixing flows, Combust. Flame 109 (1–2) (1997) 198–223.